IEEE Access
Multidisciplinary ⋮ Rapid Review ⋮ Open Access Journal

Received 13 April 2026, accepted 29 April 2026, date of publication 6 May 2026, date of current version 11 May 2026.

Digital Object Identifier 10.1109/ACCESS.2026.3690910

RESEARCH ARTICLE

Distributed Reactive Power Control With Adaptive Volt/VAr in Active Distribution Systems

HILAL OZDEMIR[1,2], A. SELIM TURKOGLU[3], OZAN ERDINÇ[4], (Senior Member, IEEE), AND IOANA PISICA[1], (Senior Member, IEEE)

[1]Electronic and Electrical Engineering Department, Brunel University of London, UB8 3PH London, U.K.
[2]UK Power Networks DSO, SE1 6NP London, U.K.
[3]Electrical and Computer Engineering Department, University of Porto, 4099-002 Porto, Portugal
[4]Electrical Engineering Department, Yıldız Technical University, 34220 Istanbul, Türkiye

Corresponding author: Hilal Ozdemir (hilal.ozdemir@brunel.ac.uk)

The work of Hilal Ozdemir was supported by the Engineering and Physical Sciences Research Council (EPSRC) under Grant EP/W524542/1.

ABSTRACT The rapid development of distributed generators (DGs) has increased the complexity of distribution system (DS), creating a need for advanced solutions to maintain operational constraints. This paper introduces a novel distributed decision-making algorithm that models DS operators and DGs as distinct entities, addressing the growing complexity of DSs while accounting for realistic operational constraints. The proposed approach utilizes the reactive power support of DGs to minimize energy curtailment through an adaptive piecewise Voltage/Reactive Power (Volt/VAr) control strategy. The proposed algorithm is tested on both the IEEE 33-bus test system and a real-world distribution network, which includes an existing battery-based energy storage system (BESS) and is extended with an electrolyzer to capture additional operational flexibility. This is achieved using Mixed-Integer Nonlinear Programming (MINLP) modeling, which identifies dynamic operating regions for smart inverters and ensures compliance with network requirements. This study contributes to the existing knowledge by addressing network complexity via modeling the DS operator and DGs as distinct entities, considering real-world limitations and privacy concerns, while also providing an adaptive Volt/VAr control strategy to enhance network performance and DG integration. The effectiveness of the proposed algorithm is demonstrated by a significant reduction in active power curtailment compared to default voltage settings.

INDEX TERMS Distributed optimization, inverter-based resources, multi-agent systems, Volt/VAr control.

NOMENCLATURE

The sets, parameters, and variables are stated below.

SETS

$\mathcal{I}$	Set of all buses in the distribution network.
$\mathcal{K}$	Set of iteration numbers.
$\mathcal{N}$	Set of all sub-problems or agents.
$\mathcal{P}$	Set of DGs.
$\mathcal{S}$	Set of slack buses.
$\mathcal{T}$	Set of time periods.
χ	Set of DSO-side local copies of coupling variables.
$\mathcal{B}$	Set of BESS.
$\mathcal{E}$	Set of electrolyzers.
$\mathcal{V}$	Set of tube trailers.
$\mathcal{Z}$	Set of DG-side local copies of coupling variables.
Ω_l^i	Set of buses connected to bus i associated with line l.

PARAMETERS

α	Coefficient for penalty parameter update.
η_i^{inv}	Efficiency of the inverter of the PV system at bus i.
η_i^{elc}	Power-to-kilogram ratio of electrolyzer at bus i [kg/MW].
CE	Charging efficiency of BESS at bus i.
DE	Discharging efficiency of BESS at bus i.
ϵ	Small coefficient.
$m_i^{h-ess_{init}}$	Initial hydrogen level in the HSU at bus i.

The associate editor coordinating the review of this manuscript and approving it for publication was Xiaodong Liang.

$m_i^{h-ess_{min}}$ Minimum allowable hydrogen in the HSU at bus i.
$m_{v,i}^{h_{arr}}$ Hydrogen level of tube trailer v upon arrival.
$m_{v,i}^{h_{des}}$ Desired hydrogen level of tube trailer v.
M Large coefficient.
$P_{i,t}^{d}$ Active power demand of bus i in period t [pu].
$\overline{P}^{\text{slack}}$ Maximum active power generation from the slack bus [MW]/[pu].
$Q_{i,t}^{d}$ Reactive power demand of bus i in period t [pu].
$\overline{Q}_i^{\text{slack}}$ Maximum reactive power generation from the slack bus [MW]/[pu].
$\overline{q}$ Maximum allowable reactive power injection limit.
$\underline{q}$ Minimum allowable reactive power injection limit.
$R_{i,j}$ Resistance of branch (i,j) [pu].
SoE_i^{max} Maximum state-of-energy for the BESS at bus i.
SoE_i^{min} Minimum state-of-energy for the BESS at bus i.
t^{init} Initial time of the simulation period.
$t_{v,i}^{arr}$ Arrival time of tube trailer v at bus i.
$t_{v,i}^{dep}$ Departure time of tube trailer v from bus i.
ρ Penalty parameter.
V_{nom} Nominal voltage.

VARIABLES

$m_{i,t}^{h,prod}$ Hydrogen produced at bus i and time t.
$m_{i,t}^{h\text{-}ess}$ Hydrogen stored in the HSU at bus i and time t [kg].
$m_{v,i,t}^{h,S2T}$ Hydrogen transmitted from HSU to tube trailer v at time t.
$P_{i,t}^{char}$ Active power used for charging the BESS at bus i and time t [pu].
$P_{i,t}^{dchar}$ Active power used for discharging the BESS at bus i and time t [pu].
$P_{i,k,t}^{DS}$ Active power decision of DS operator at iteration k.
$P_{i,k,t}^{DG}$ Active power decision of DG i at iteration k and time t.
$P_{i,t}^{elc}$ Active power consumed by the electrolyzer at bus i and time t.
$P_{i,t}^{flex}$ Flexible demand connected at bus i and time t.
$P_{i,t}^{G2E}$ Active power transferred from the grid to the electrolyzer at bus i and time t.
$P_{i,t}^{PV\text{-}curt}$ Curtailed active power of the PV at bus i and time t [pu].
$P_{i,t}^{PV2E}$ Active power supplied from PV to the electrolyzer at bus i and time t.
$P_{i,j,t}^{loss}$ Active power loss along the line between bus i and j at time t [pu].
$P_{i,t}^{g}$ Total active power transferred from the substation bus i in period t [pu].
$P_{i,j,t}^{f}$ Active power flow of branch (i,j) in period t [pu].
$P_{i,t}^{slack}$ Active power supplied from the slack bus at time t.
$Q_{i,j,t}^{f}$ Reactive power flow of branch (i,j) in period t [pu].
$Q_{i,j,t}^{loss}$ Reactive power losses of branch (i,j) in period t [pu].
$Q_{i,t}^{g}$ Total reactive power transferred from the substation bus i in period t [pu].
$Q_{i,k,t}^{DS}$ DS operator reactive power decision at iteration k.
$Q_{i,k,t}^{DG}$ DG reactive power decision at iteration k.
$v_{i,t}$ Voltage of bus i in period t [pu].
$v_{1-4,t}$ Volt/VAr control setpoint voltages in period t [pu].
$u_{v_{1-4},t}$ Binary variables for the setpoint area selection in period t.
$u_{i,t}^{char}$ Binary variable; 1 if the BESS at bus i is charging at time t, otherwise 0.
$u_{i,t}^{elc}$ Binary variable; 1 if electrolyzer demand at bus i is met via PV-to-grid route, otherwise from the grid.
$\lambda_{i,k,t}^{p}$ Dual variable for the active power of DG bus i in period t at iteration k.
$\lambda_{i,k,t}^{q}$ Dual variable for the reactive power of DG bus i in period t at iteration k.
σ_k Penalty coefficient for the local equality boundary conditions.

I. INTRODUCTION

A. MOTIVATION

The growing urgency to address greenhouse gas emissions, in alignment with commitments under the Paris Agreement, has positioned distributed generators (DGs) as a pivotal solution for decarbonizing the power sector. However, the intermittent nature, location-specific challenges, and unpredictability of DGs introduce significant operational concerns. These include breaches of operational thresholds, voltage fluctuations, and power quality issues within distribution systems (DSs). Effectively addressing these challenges requires the development and deployment of advanced control techniques to mitigate their negative impacts.

Among the promising solutions, the reactive power support of inverter-based resources such as DGs stand out as an effective mechanism to alleviate these issues. Industrial projects have demonstrated the potential of reactive power support to enhance network performance [1], [2] For instance, one project [1] explored the use of reactive power from inverter-based technologies, including photovoltaics (PVs), to align with the UK's ambitious net-zero targets. Similarly, the Power Potential Project [3] leveraged DG reactive power to manage voltage and thermal constraints, thus reducing the need for costly network reinforcements. Another study [2] demonstrated the ability of reactive power support to enhance network stability and reliability within a short project

span. These examples underscore how reactive power not only mitigates operational challenges, such as voltage limit violations, but also offers cost savings for customers by reducing infrastructure reinforcement requirements [4].

Smart inverters enable the deployment of various reactive power control techniques, which can operate based on voltage, active power, or a constant reactive power mode [5]. Among these techniques, Voltage/Reactive Power (Volt/VAr) control stands out as an effective approach to address voltage limit violations by dispatching reactive power based on the measured voltage levels. However, despite its advantages, reactive power support must be carefully managed to prevent unintended consequences, such as increased power losses within the network [6]. This underscores the importance of developing efficient control techniques to optimize reactive power utilization. In addition to advanced control techniques, the integration of flexibility sources plays a key role in addressing the challenges associated with high DG penetration. Energy storage systems, deployed by both DS operators and end users, provide short-term operational flexibility, while hydrogen emerges as a promising long-duration energy carrier with storage capability. In this context, the integration of additional flexibility sources, such as hydrogen as an emerging energy carrier and battery-based energy storage systems (BESSs), provides new opportunities to enhance network operation. These technologies complement reactive power control by offering both short- and long-term flexibility, enabling more efficient energy management and supporting the accommodation of high renewable penetration. Motivated by these challenges and opportunities, numerous studies have proposed advanced control algorithms that utilize the reactive power capabilities of DGs through Volt/VAr strategies, aiming to minimize operational constraint violations in DSs.

B. LITERATURE REVIEW

Reactive power control techniques can be divided into three main categories based on their communication structure as centralized, distributed, and local approaches. Centralized control systems consolidate decision-making into a single central structure, utilizing global information to optimize performance of the entire system. Distributed control systems strike a balance by dividing the primary problem into smaller sub-problems, each handled by a subset of controllers. These controllers make decisions based on local information while collaborating with one another to achieve overarching system objectives.

Majority of the current literature focuses on centralized approaches for reactive power control of inverter-based resources and optimal power allocation across the entire network. For example, [7] proposes a mixed-integer linear programming model to achieve proportional reactive power sharing among DGs while minimizing line losses in a droop-based micro-grid. Similarly, [8] presents a convex second-order cone programming-based AC optimal power flow (OPF) model for three-phase unbalanced DSs. This model incorporates smart inverters and Volt/VAr controllers, characterizing the reactive power-voltage behaviour of smart inverters and co-optimizing the Q-V characteristics of Volt/VAr control to ensure system stability through dynamic analyses. Despite their advantages, centralized approaches in DSs, where a single controller, typically the DS operator, oversees the entire system, including DG control, face significant limitations. These include vulnerability to incomplete or inaccurate information at any point in the network and the impracticality of direct DS operator control over DGs beyond their network connection. These challenges underline the need for alternative and more decentralized, mainly distributed strategies, to provide global solution.

Such distributed approaches decompose the main problem into smaller sub-problems, each solved independently. To achieve a global optimal solution, only limited information is exchanged between subsets of these sub-problems. Additionally, distributed optimization enhances robustness by ensuring the system can tolerate the failure of individual agents. It also preserves privacy by minimizing the need for extensive information sharing across the entire network. Studies such as [9] and [10] provide comprehensive reviews of distributed optimization methods in power systems, highlighting their benefits and various use cases in the literature. These advantages have driven a growing research focus on distributed approaches in reactive power control in power systems rich in inverter-based resources.

Numerous studies in the literature propose distributed optimization methods for reactive power control, considering the minimum and maximum reactive power support capabilities of inverter-based resources. For instance, [11] decomposes the distribution system into multiple areas to minimize network losses, while [12] integrates column-and-constraint generation with Alternating Direction Method of Multipliers (ADMM) to handle the non-convex Volt/VAr problem and improve convergence. Similarly, [13] models each node as an independent agent in low-voltage systems to reduce grid power exchange, and [14] introduces a robust online Volt/VAr control formulation with a regularized Lagrangian to enhance convergence stability. In addition, [15] incorporates long short-term memory to accelerate ADMM by regressing primal and dual variables, while [16] proposes an accelerated ADMM framework targeting loss and voltage deviation minimization. The approach in [17] employs a consensus-based secondary controller for wind turbines; however, coordination is limited to wind plants and does not extend to the broader distribution system. These studies demonstrate efficient distributed optimization solutions for reactive power control, leveraging the reactive power capabilities of DGs to address challenges in power systems. However, they only consider the minimum and maximum limits for reactive power control mechanisms. This limitation can lead to excessive reactive power penetration, which may cause significant issues, such as increased power losses and the need for costly network reinforcements.

In addition to the proposed advanced techniques, standards have been introduced to ensure the interoperability of inverter-based resources. Among them, the IEEE standard 1547 plays a pivotal role in providing a framework for piecewise Volt/VAr control that considers the reactive power capacity of inverters. It has been widely adopted in several countries, including the USA [18], Thailand, and Vietnam [19]. The standard specifies voltage set points for Volt/VAr control and defines adjustable ranges for these settings, allowing for flexibility in implementation. In [20], an incremental Volt/VAr control approach is applied to low-voltage DSs, adopting the recommended voltage settings. However, when voltage violations occur, the reactive power of each DG is adjusted based on their sensitivity factors rather than following the incremental Volt/VAr control mechanism. The optimization of Volt/VAr control settings and its effect in DS are explored in [21] and [22]. In [21], a genetic algorithm is proposed to minimize voltage deviation, power loss, and peak reactive power. The settings for the Volt/VAr rule are adjusted seasonally for summer and winter. The results indicate that while only adjusting the dead band minimizes power loss, modifying both the voltage set points and reactive power yields the smallest voltage deviation. In [22], the effects of piecewise Volt/VAr settings are tested on a real DS, the Maui Smart Grid in Hawaii. By varying the voltage settings, the inductive and capacitive behaviour of Volt/VAr control is observed. The findings demonstrate that employing Volt/VAr control effectively mitigates voltage violations. Moreover, the voltage settings significantly influence the reactive power absorbed or injected by inverters and the DS transformer.

There are some studies considering other flexibility technologies along with Volt/VAr control, where allocation of the demand and operation of BESS of prosumers are considered in addition to the Volt/VAr control of PVs [23]. A reactive power allocation algorithm is developed for distribution networks incorporating electrolyzer connections and BESS in [24]. Reference [25] proposes a decentralized framework that partitions the distribution network into multiple sections, enabling the integration of hydrogen-based energy storage systems for effective voltage regulation. In [26],the reactive power capability of electric vehicles is utilized for voltage regulation within a centralized framework; however, the approach does not account for the reactive power contribution of PV systems.

Given the critical importance of voltage settings for reactive power control, more advanced methodologies have emerged in the recent literature. For instance, [27] and [28] propose deep learning-based approaches for Volt/VAr control, showcasing the potential for enhanced performance in managing reactive power in modern DSs. Reference [29] proposes a data-driven approach for Volt/VAr control in PV-integrated distribution networks. The network is partitioned into multiple zones, with a dedicated zone controller assigned to each zone to coordinate the operation of multiple PV units. A multi-agent reinforcement learning framework is proposed for distributed Volt/VAr control, where a centralized training phase is employed prior to the deployment of decentralized control strategies [30].

C. CONTRIBUTION AND ORGANIZATION

The literature clearly highlights the critical role of reactive power support from DGs in addressing significant challenges in DSs, such as voltage violations and power losses. This study proposes a distributed optimization-based decision-making algorithm that dynamically designs piecewise Volt/VAr control rules while considering the complexity and realistic limitations of the modern DSs. Recognizing the limitation that DSOs have no direct control over DGs beyond their connectivity, the network is decomposed into sub-problems, represented by distinct agents—namely, the DG owners and the DS operator—each with its own objective functions. Each sub-problem is solved independently while accounting for interdependencies through dual variables. The distributed solution is achieved using the ADMM, ensuring a coordinated approach that respects the individual objectives of the agents and addresses the interconnected nature of the DS.

The contributions of this study can be summarized as follows:

- A distributed decision-making algorithm is proposed in which the DS operator and DG owners are distinctly modeled with their own objectives while effectively addressing the boundaries and interactions between these entities. While a limited number of studies have explored similar distributed frameworks, existing approaches do not explicitly model the DSO and DGs as independent stakeholders with distinct objectives under practical operational constraints. This distinction is crucial for incorporating real-world limitations, such as the lack of direct control by the DS operator over DG operations and the increasing complexity of DSs as the number of DG connections continues to grow.
- An adaptive piecewise Volt/VAr control strategy is proposed for the reactive power support of DGs, where voltage set points are dynamically dispatched within a holistic framework to effectively address breaches of operational constraints in the DS Unlike conventional approaches, the Volt/VAr parameters are determined in a distributed manner, enabling scalable and privacy-preserving coordination among network agents.
- The reactive power support of DGs is executed with a new curtailment minimization oriented approach where their Volt/VAr settings are dispatched to achieve this objective, thereby enhancing their penetration into the DS.
- To demonstrate the robustness of the proposed algorithm, it was tested on a real distribution network. Also, this distribution network was further extended with electrolyzer connection to reflect the future distribution network network behaviour by considering a new energy carrier, hydrogen.

The reminder of the study is organized as follows: Section II provides the mathematical background of the framework. Section III outlines the anticipated outcomes of the proposed management strategy. Finally, Section IV presents the concluding remarks and offers suggestions for future research.

II. PROPOSED CONTROL STRATEGY

A. ADAPTIVE PIECEWISE VOLT/VAr CONTROL STRATEGY

Volt/VAr control plays a critical role in mitigating voltage limit violations caused by the high penetration of DGs and in reducing the energy curtailment of these generators. Piecewise Volt/VAr control, as illustrated in Fig. 1, establishes the relationship between reactive power and voltage at the point of connection, ensuring that voltage levels remain within operational limits. Voltage settings are crucial for efficient reactive power control, and the IEEE standard 1547 defines voltage setting ranges that consider the interoperability of DGs with the grid. Reactive power dispatch can be achieved by tuning five parameters: v_1, v_2, v_3, v_4, and v_{ref}. Among these parameters, v_1 and v_4 represent the minimum and maximum operating voltage limits, respectively. The parameter v_{ref} defines the optimal voltage level, while v_2 and v_3 allow for extended operation to support grid stability. The IEEE standard 1547 also provides default voltage settings where reference voltage is set equal to nominal voltage and voltage settings are defined as $v_1 = \hat{v} - 0.08\,\tilde{v}$, $v_2 = \hat{v} - 0.02\,\tilde{v}$, $v_3 = \hat{v} + 0.02\,\tilde{v}$, $v_4 = \hat{v} + 0.08\,\tilde{v}$.

The proposed adaptive Volt/VAr control dynamically fine-tunes these parameters and the control rules for Volt/VAr control are provided in Eqs. (1)-(7). Voltage settings are adaptable within the ranges outlined in Eqs. (1)-(5) with nominal and reference voltages denoted as $\tilde{v}$, and $\hat{v}$, respectively. The inverter switches to injection mode when voltage drops below v_2, while it transitions to absorption mode when voltage exceeds v_3. The upper and lower limits for reactive power injection are defined in Eq. (6) and Eq. (7), where $\tilde{s}$ represents the nameplate apparent power.

$$0.95\,\tilde{v} \le \hat{v} \le 1.05\,\tilde{v} \tag{1}$$

$$\hat{v} - 0.18\,\tilde{v} \le v_1 \le v_2 - 0.02\,\tilde{v} \tag{2}$$

$$\hat{v} - 0.03\,\tilde{v} \le v_2 \le \hat{v} \tag{3}$$

$$\hat{v} \le v_3 \le \hat{v} + 0.03\,\tilde{v} \tag{4}$$

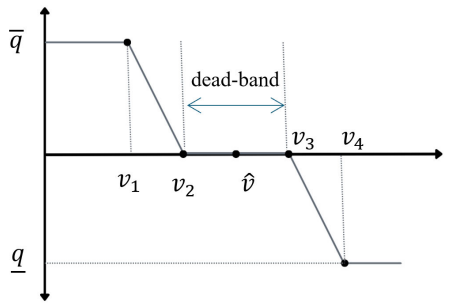

FIGURE 1. Piecewise Volt/VAr control curve with adjustable voltage settings.

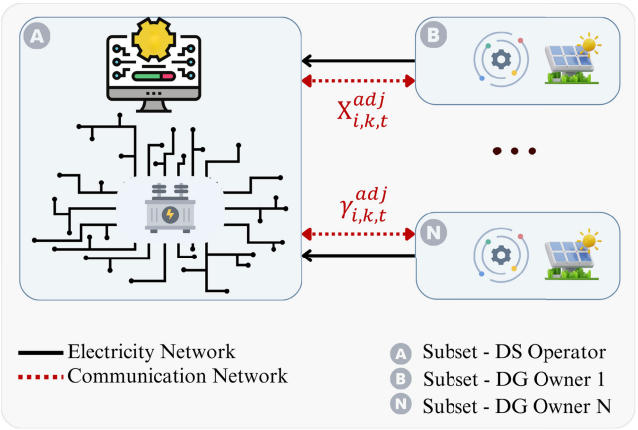

FIGURE 2. Proposed strategy illustrating power and communication interaction between DS operator and DGs.

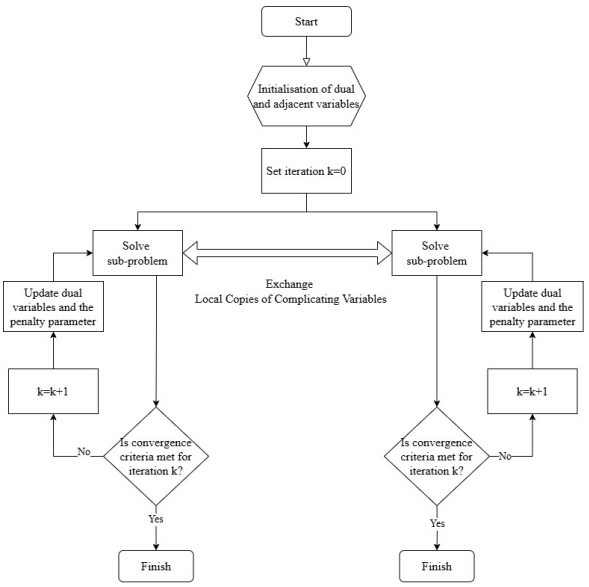

FIGURE 3. Iteration process of the proposed distributed optimization algorithm.

$$v_3 + 0.02\,\tilde{v} \le v_4 \le \hat{v} + 0.18\,\tilde{v} \tag{5}$$

$$\overline{q} = 0.44\,\tilde{s} \tag{6}$$

$$\underline{q} = -0.44\,\tilde{s} \tag{7}$$

B. CONSENSUS-BASED DISTRIBUTED NETWORK MODEL WITH ADAPTIVE VOLT/VAr CONTROL

The increasing number of inverter-based resources connected to the DS significantly enhances its complexity. Given this growing complexity and the fact that DS operators have no direct control over DGs beyond their connectivity, this study proposes a decomposition of the DS into sub-problems. By employing ADMM, the DS operator and DGs are modeled as distinct sub-problems with their own objective functions and constraints, allowing for a more effective and decentralized approach to manage the network.

As illustrated in Fig. 2, the DS is partitioned into $\mathcal{N}$ subsets, with each subset defined by its local variables and

constraints. Variables that link two subsets, referred to as complicating variables, are locally represented by adjacent variables for coordination purposes. These local representations are denoted as $\chi^{adj}_{i,k,t}$ for the DS subset, and $\gamma^{adj}_{i,k,t}$ for the DG subsets. Each subset solves its own optimization problem independently, using its specific objectives and local variables. Once the local optimization is completed, adjacent variables are shared with neighbouring subsets. To ensure the distributed optimization algorithm achieves the overall objective of the DS, the adjacent variables in each subset must align with those in neighbouring subsets. This consistency is enforced through iterative updates, allowing the adjacent variables to converge toward a common solution over successive iterations. The flow chart in Fig. 3 illustrates the iteration process of the proposed algorithm, showing the key steps from local optimization to convergence.

The partitioning of the DS into DS operator and DG subsets introduces active and reactive power flow as complicating variables between the two. The complicating variables for the DS operator subset are defined in Eq. (8), while those for the DG subsets are provided in Eq. (9). Achieving global optimization requires that the adjacent variables in the DS operator and DG subsets be equal, ensuring coordination across the entire network as given in Eqs. (10) and (11).

$$\chi^{adj}_{i,k,t} = \{P^{DS}_{i,k,t}, Q^{DS}_{i,k,t}\} \tag{8}$$

$$\gamma^{adj}_{i,k,t} = \{P^{DG}_{i,k,t}, Q^{DG}_{i,k,t}\} \tag{9}$$

$$P^{DS}_{i,k,t} = P^{DG}_{i,k,t} \tag{10}$$

$$Q^{DS}_{i,k,t} = Q^{DG}_{i,k,t} \tag{11}$$

1) OBJECTIVE FUNCTION

The objective of the main problem consists of two components, as given in Eq. (12). The first term represents the objective of the DS operator, which is to minimize total power losses within the network. The second term corresponds to the objective of the DGs, namely the minimization of total curtailment in their active power injection.

$$\mathcal{F}(x,z) = \sum_{i,j,t} P^{loss}_{i,j,t} + \sum_{i,t} P^{PV-curt}_{i,t} \tag{12}$$

2) LAGRANGIAN FUNCTION

Replacing the coupling variables with their local copies enables the decoupling of the DSO and DG models, apart from the constraints defined in Eq. (10) and Eq. (11), where the local copies must be equal. These equality constraints re-establish coupling between the DS operator and DG subsets. However, they can be effectively addressed by incorporating them into the Lagrangian function through the introduction of dual variables. The Lagrangian function for the problem is defined in Eq. (13). The first term represents the objective of the DS operator and DGs. The dual variables λ enforce the coupling constraints by penalising the discrepancy between the duplicated local variables. The parameter σ introduces a penalty term that enhances robustness, as it remains differentiable under relatively mild conditions [31].

$$\begin{aligned}\mathcal{L}(x,z) = \mathcal{F}(x,z) &+ \sum_{i,t}\left[\lambda^{p}_{i,t}\left(P^{\mathrm{DG}}_{i,t} - P^{\mathrm{DS}}_{i,t}\right) + \frac{\rho}{2}\left(P^{\mathrm{DG}}_{i,t} - P^{\mathrm{DS}}_{i,t}\right)^2\right] \\ &+ \sum_{i,t}\left[\lambda^{q}_{i,t}\left(Q^{\mathrm{DG}}_{i,t} - Q^{\mathrm{DS}}_{i,t}\right) + \frac{\rho}{2}\left(Q^{\mathrm{DG}}_{i,t} - Q^{\mathrm{DS}}_{i,t}\right)^2\right].\end{aligned} \tag{13}$$

3) SUBSET–DS OPERATOR

DS is modelled as Mixed-Integer Quadratically Constrained Program and the OPF equations are shown in (14)-(25). Equations (14) and (19) represent the active and reactive power flows in the system, respectively. In Eq. (14), the right-hand side captures the total network demand, including electrolyzer load and power losses, whereas the left-hand side represents the available supply from local generation and BESS resources. The second and third terms on the left-hand side denote the incoming and outgoing power flows, respectively. The nonlinear power losses for active and reactive power are defined in Eqs. (15) and (21), respectively. Power generation at a bus is restricted to the slack and DG buses and this constraint is ensured via Eq. (16). For the slack bus, the total power is supplied by the slack source. If a bus accommodates an electrolyzer or a BESS alongside a PV system, the generation is defined by the PV output. For buses hosting standalone PV systems, generation is represented by the corresponding local decision variable. At all other buses, no active power generation is permitted. Eq. (17) represents the power demand of the electrolyzer, provided there is a connection at the corresponding bus. The net power of the BESS is defined in Eq. (18). When an BESS is present at bus i, it is defined as the difference between charging and discharging power. Positive values indicate discharging, while negative values represent charging. The reactive power supply is limited to the slack bus and standalone DG units, where standalone PVs denote PV systems operating independently without associated ESS or electrolyzer connections, as defined in Eq. (20).

$$\begin{aligned}&P^{g}_{i,t} + \sum_{i\Omega^{j}_{l}} P^{f}_{i,j,t} - \sum_{j\Omega^{i}_{l}} P^{f}_{j,i,t} + P^{BESS}_{i,t} \\ &= P^{loss}_{i,j,t} + P^{d}_{i,t} + P^{flex}_{i,t} \quad \forall i,j \in \mathcal{I},\ t \in \mathcal{T}\end{aligned} \tag{14}$$

$$P^{loss}_{i,j,t} = R_{i,j} \cdot \frac{{P^{f}_{i,j,t}}^2 + {Q^{f}_{i,j,t}}^2}{V^2_{nom}} \quad \forall i,j \in \mathcal{I}, t \in \mathcal{T} \tag{15}$$

$$P^{g}_{i,t} = \begin{cases} P^{slack}_{i,t} & i \in \mathcal{S}, \forall t \in \mathcal{T} \\ P^{DS}_{i,t} & i \in \mathcal{P} - \{\mathcal{B}, \mathcal{E}\}, \forall t \in \mathcal{T} \\ P^{PV}_{i,t} & i \in \{\mathcal{B}, \mathcal{E}\}, \forall t \in \mathcal{T} \\ 0 & i \notin \{\mathcal{S}, \mathcal{P}\}, \forall t \in \mathcal{T} \end{cases} \tag{16}$$

$$P^{flex}_{i,t} = \begin{cases} P^{elc}_{i,t} & i \in \mathcal{E}, \forall t \in \mathcal{T} \\ 0 & i \notin \mathcal{E}, \forall t \in \mathcal{T} \end{cases} \tag{17}$$

$$P_{i,t}^{BESS} = \begin{cases} P_{i,t}^{char} - P_{i,t}^{dchar} & i \in \mathcal{B}, \forall t \in \mathcal{T} \\ 0 & i \notin \mathcal{B}, \forall t \in \mathcal{T} \end{cases} \tag{18}$$

$$Q_{i,t}^{g} + \sum_{i\Omega_l^j} Q_{i,j,t}^{f} - \sum_{j\Omega_l^i} Q_{j,i,t}^{f} = Q_{i,j,t}^{loss} + Q_{i,t}^{d} \quad \forall i,j \in \mathcal{I}, t \in \mathcal{T} \tag{19}$$

$$Q_{i,t}^{g} = \begin{cases} Q_{i,t}^{slack} & i \in \mathcal{S}, \forall t \in \mathcal{T} \\ Q_{i,t}^{DS} & i \in \mathcal{P} - \{\mathcal{B}, \mathcal{E}\}, \forall t \in \mathcal{T} \\ 0 & i \notin \{\mathcal{S}, \mathcal{P}\}, \forall t \in \mathcal{T} \end{cases} \tag{20}$$

$$Q_{i,j,t}^{loss} = X_{i,j} \cdot \frac{{P_{i,j,t}^{f}}^2 + {Q_{i,j,t}^{f}}^2}{V_{nom}^2} \quad \forall i,j \in \mathcal{I}, t \in \mathcal{T} \tag{21}$$

The active and reactive power generation limits at the substation bus are defined by Eqs. (22) and (23), which are set according to the transformer capacity. The voltage drop between buses is captured by Eq. (24), while Eq. (25) defines the lower and upper voltage limits at each bus.

$$0 \le P_{i,t}^{slack} \le \overline{P^{slack}}, \quad i \in \mathcal{S}, \forall t \in \mathcal{T} \tag{22}$$

$$\underline{Q^{slack}} \le Q_{i,t}^{slack} \le \overline{Q^{slack}}, \quad i \in \mathcal{S}, \forall t \in \mathcal{T} \tag{23}$$

$$V_{j,t} = V_{i,t} - 2\left(R_{ij} \cdot P_{i,j,t}^{f} + X_{ij} \cdot Q_{i,j,t}^{f}\right) \quad \{i,j\} \in \mathcal{I}, \forall t \in \mathcal{T} \tag{24}$$

$$\underline{V} \le V_{i,t} \le \overline{V} \quad i \in \mathcal{I}, \forall t \in \mathcal{T} \tag{25}$$

Hydrogen production via electrolysis depends on the supplied electrical power and the power-to-hydrogen conversion efficiency, as expressed in Eq. (26). The power demand of the electrolyzer can be met by solar generation at the corresponding bus or supplemented by the grid when solar output is insufficient, as shown in Eq. (27). Any surplus solar power, after meeting the electrolyzer's demand, can be injected into the grid, as described in Eq. (28). Eqs. (29) and (30) ensure that power is not simultaneously transferred from the PV to the grid and from the grid to the electrolyzer. The binary variable $u_{i,t}^{elc} = 1$ indicates that power flows from the PV to the grid, whereas $u_{i,t}^{elc} = 0$ signifies that grid power is being used to supply the electrolyzer.

$$m_{i,t}^{h,prod} = P_{i,t}^{elc} \cdot \eta_i^{elc}, \quad \forall i \in \mathcal{E}, t \in \mathcal{T} \tag{26}$$

$$P_{i,t}^{elc} = P_{i,t}^{G2E} + P_{i,t}^{PV2E}, \quad \forall i \in \mathcal{E}, t \in \mathcal{T} \tag{27}$$

$$P_{i,t}^{PV} = P_{i,t}^{PV2E} + P_{i,t}^{PV2G} + P_{i,t}^{PV-curt}, \quad \forall i \in \mathcal{E}, t \in \mathcal{T} \tag{28}$$

$$P_{i,t}^{PV2G} \le N \cdot u_{i,t}^{elc}, \quad \forall i \in \mathcal{E}, t \in \mathcal{T} \tag{29}$$

$$P_{i,t}^{G2E} \le N \cdot (1 - u_{i,t}^{elc}), \quad \forall i \in \mathcal{E}, t \in \mathcal{T} \tag{30}$$

The dynamics of the hydrogen storage unit (HSU) are modelled in Eq. (31). The HSU is initialized with a given hydrogen level and updated based on the balance between hydrogen produced via electrolysis and the quantity delivered to tube trailers. Capacity limits are enforced by constraints on the minimum and maximum allowable hydrogen levels, ensuring that storage remains within operational boundaries. The total amount of hydrogen supplied from the HSU to the tube trailers is defined in Eq. (32).

$$m_{i,t}^{h-ess} \begin{cases} = m_i^{h-ess_{init}}, & \forall i \in \mathcal{E}, t = t_{init} \\ = m_{i,t-1}^{h-ess} + m_{i,t}^{h,prod} - m_{i,t}^{h,S2T_{tot}}, & i \in \mathcal{E}, t \in \mathcal{T} - \{t_{init}\} \\ \le m_i^{h-ess_{max}}, & \forall i \in \mathcal{E}, t \in \mathcal{T} \\ \ge m_i^{h-ess_{min}}, & \forall i \in \mathcal{E}, t \in \mathcal{T} \end{cases} \tag{31}$$

$$m_{i,t}^{h,S2T_{tot}} = \sum_{T} m_{v,i,t}^{h,S2T}, \quad \forall i \in \mathcal{E}, v \in \mathcal{V}, t \in \mathcal{T} - \{t_{init}\} \tag{32}$$

The hydrogen transfer to tube trailers and the associated operational constraints are formulated in Eq. (33). Each trailer is initialized with a predefined quantity of hydrogen and must depart with a specified target level. The hydrogen content of each trailer increases through supply transactions from either electrolyzer production or the storage system.

$$m_{v,i,t}^{h} = \begin{cases} m_{v,i}^{h_{arr}}, & t = t_{v,i}^{arr} \\ m_{v,i}^{h_{des}} & t = t_{v,i}^{dep} \\ m_{v,i,t-1}^{h} + m_{i,t}^{h,prod} + m_{v,i,t}^{h,S2T} & t_{v,i}^{arr} \le t \le t_{v,i}^{dep} \end{cases} \tag{33}$$

The BESS is described by the state-of-energy balance in Eq. (34). At the start of the simulation the battery is set to its minimum state-of-energy, and throughout the optimization horizon its state-of-energy is forced to remain within the prescribed lower and upper limits. The state-of-energy rises when the battery is charging and falls when it is discharging. Maximum charge and discharge rates are enforced by Eqs. (35) and (36), and an additional binary constraint prevents the battery from charging and discharging in the same time step.

$$SoE_{i,t} \begin{cases} = SoE_i^{min}, & \forall i \in \mathcal{B},\ t = t^{init} \\ \le SoE_i^{max}, & \forall i \in \mathcal{B},\ t \in \mathcal{T} \\ \ge SoE_i^{min}, & \forall i \in \mathcal{B},\ t \in \mathcal{T} \\ = SoE_{i,t-1} + \left(P_{i,t}^{char} \cdot CE \cdot \Delta T\right) & \\ \quad - \left(\dfrac{P_{i,t}^{dchar} \cdot \Delta T}{DE}\right) & \forall i \in \mathcal{B}, \\ t \in \mathcal{T} \setminus \{t^{init}\} & \end{cases} \tag{34}$$

$$P_{i,t}^{char} \le CR_i \cdot u_{i,t}^{char}, \quad \forall i \in \mathcal{B}, t \in \mathcal{T} \tag{35}$$

$$P_{i,t}^{dchar} \le DR_i \cdot \left(1 - u_{i,t}^{char}\right) \quad \forall i \in \mathcal{B}, t \in \mathcal{T} \tag{36}$$

4) SUBSETS—DGs

The equations for the DGs are shown in (38)-(46). The apparent power output of PV systems depends on the inverter's efficiency in converting generated solar power, as expressed in Eq. (37). According to (38), the instantaneous apparent power generated by the DG can be injected into the grid either as active or reactive power, or can be curtailed. Based on the Volt/VAr control, the DG inverter can operate in

an inductive mode if voltage is high and draw reactive power from the grid.

$$S_{i,t}^{PV} = P_{i,t}^{PV_{gen}} \cdot \eta_i^{inv}, \quad i \in \mathcal{P}, \forall t \in \mathcal{T} \tag{37}$$

$$S_{i,t}^{PV^2} = \left(P_{i,t}^{DG} + P_{i,t}^{PV-curt}\right)^2 + Q_{i,t}^{DG^2} \quad i \in \mathcal{P}, \forall t \in \mathcal{T} \tag{38}$$

The voltage settings, represented by Eqs. (1)-(7), are adjusted based on the Eqs. (39)-(41). According to these equations, if the voltage exceeds v_3, the DG operates in reactive power absorption mode, and if it falls below v_2, it operates in reactive power injection mode. When the voltage remains between these two levels, the DG unit does not interact with the grid in terms of reactive power. The parameters v_2 and v_3 are dynamically adjusted at each time to minimize active power curtailment.

$$Q_{i,t}^{DG} \leq 0 \; if \; V_{i,t} \geq v_{3,t} \quad i \in \mathcal{P} - \{\mathcal{B}, \mathcal{E}\}, \forall t \in \mathcal{T} \tag{39}$$

$$Q_{i,t}^{DG} \geq 0 \; if \; V_{i,t} \leq v_{2,t} \quad i \in \mathcal{P} - \{\mathcal{B}, \mathcal{E}\}, \forall t \in \mathcal{T} \tag{40}$$

$$Q_{i,t}^{DG} = 0 \; if \; \; v_{2,t} \leq V_{i,t} \leq v_{3,t} \quad i \in \mathcal{P} - \{\mathcal{B}, \mathcal{E}\}, \forall t \in \mathcal{T} \tag{41}$$

The conditional statements including reactive power control introduce discontinuities and non-linearities. To handle these discontinuities, a mixed-integer linear programming formulation is required for the equations in (39)–(41). Accordingly, these equations have been reformulated into a mixed-integer linear programming model, as shown in (42)–(46), by introducing binary variables, big-M notation, and indicator constraints.

According to the reformulated equations, if the voltage at the DG bus exceeds v_3, the binary variable u_{v_3} is activated. Conversely, if the voltage is below v_2, the binary u_{v_2} is activated. Based on these binary states, the reactive power injection or absorption decisions are determined through indicator constraints. The binary condition ensuring the appropriate deadband, which applies when the voltage lies between v_2 and v_3 is defined in Eq. (46). The deadband is only active when neither u_{v_2} or u_{v_3} is activated, which is enforced by setting the sum of these binary variables to zero. This formulation ensures precise control of the reactive power support under varying voltage conditions.

$$v_{i,t} \geq v_{3,t} - \mathcal{M} \cdot (1 - u_{v_3,t}) \tag{42}$$

$$v_{i,t} \leq v_{3,t} + \mathcal{M} \cdot u_{v_3,t} \tag{43}$$

$$v_{i,t} \geq v_{2,t} - \mathcal{M} \cdot u_{v_2,t} \tag{44}$$

$$v_{i,t} \leq v_{2,t} + \mathcal{M} \cdot (1 - u_{v_2,t}) \tag{45}$$

$$u_{v_{db},t} = u_{v_2,t} + u_{v_3,t} \tag{46}$$

5) ITERATIVE PROCESS

Distributed optimization begins by assigning initial values to the local variables at the first iteration. Once the local variables have been computed, each agent exchanges its updated values with neighbouring agents in preparation for the next iteration. The local variables are then updated according to Eqs. (47) and (48). Subsequently, the dual

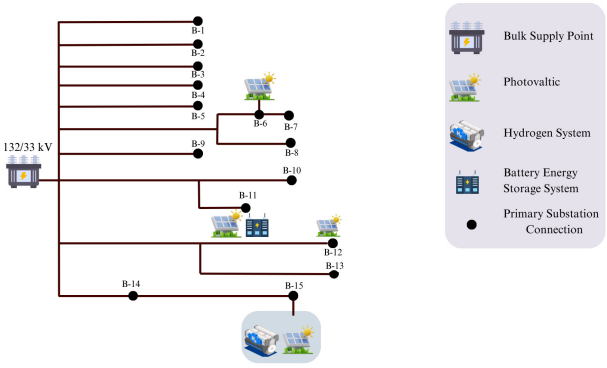

FIGURE 4. Modified Braintree distribution network topology: bulk supply point to primary substation.

variables are adjusted based on the discrepancies between the updated values in adjacent subsets, as defined in Eqs. (49) and (50). The boldface terms in Eqs. (47) and (48) indicate the local variables that are computed and updated within the update equations.

$$\begin{aligned}\mathbf{x}^{k+1} &:= \arg\min_{\mathbf{x}\in\mathcal{X}} \; \mathcal{L}\left(\mathbf{x}, z^k, \lambda^k\right) \\ &= \arg\min_{\mathbf{x}\in\mathcal{X}} \; F(\mathbf{x}) + \sum_{i,t}\Big(\lambda_{i,t}^{p,k}\left(P_{i,t}^{\mathrm{DG},k} - \mathbf{P_{i,t}^{DS}}\right) \\ &\quad + \frac{\rho^k}{2}\left(P_{i,t}^{\mathrm{DG},k} - \mathbf{P_{i,t}^{DS}}\right)^2\Big) \\ &\quad + \sum_{i,t}\Big(\lambda_{i,t}^{q,k}\left(Q_{i,t}^{\mathrm{DG},k} - \mathbf{Q_{i,t}^{DS}}\right) \\ &\quad + \frac{\rho^k}{2}\left(Q_{i,t}^{\mathrm{DG},k} - \mathbf{Q_{i,t}^{DS}}\right)^2\Big).\end{aligned} \tag{47}$$

$$\begin{aligned}\mathbf{z}^{k+1} &:= \arg\min_{\mathbf{z}\in\mathcal{Z}} \; \mathcal{L}(x^{k+1}, \mathbf{z}, \lambda^k) \\ &= \arg\min_{\mathbf{z}\in\mathcal{Z}} \; F(\mathbf{z}) + \sum_{i,t}\Big(\lambda_{i,t}^{p,k}\left(\mathbf{P}_{i,t}^{\mathrm{DG}} - P_{i,t}^{\mathrm{DS},k+1}\right) \\ &\quad + \frac{\rho^k}{2}\left(\mathbf{P}_{i,t}^{\mathrm{DG}} - P_{i,t}^{\mathrm{DS},k+1}\right)^2\Big) \\ &\quad + \sum_{i,t}\Big(\lambda_{i,t}^{q,k}\left(\mathbf{Q}_{i,t}^{\mathrm{DG}} - Q_{i,t}^{\mathrm{DS},k+1}\right) \\ &\quad + \frac{\rho^k}{2}\left(\mathbf{Q}_{i,t}^{\mathrm{DG}} - Q_{i,t}^{\mathrm{DS},k+1}\right)^2\Big).\end{aligned} \tag{48}$$

$$\lambda_{i,t}^{p,k+1} = \lambda_{i,t}^{p,k} + \rho^k\left(P_{i,t}^{\mathrm{DG},k+1} - P_{i,t}^{\mathrm{DS},k+1}\right) \tag{49}$$

$$\lambda_{i,t}^{q,k+1} := \lambda_{i,t}^{q,k} + \rho^k\left(Q_{i,t}^{\mathrm{DG},k+1} - Q_{i,t}^{\mathrm{DS},k+1}\right) \tag{50}$$

$$\rho^{k+1} := \alpha * \rho^k \tag{51}$$

6) CONVERGENCE AND STOPPING CRITERIA

The stopping criteria are defined in terms of the primal and dual residuals over successive iterations. The primal residual measures the degree of constraint violation, whereas the dual residual reflects the satisfaction of the dual feasibility condition. The expressions for the primal and dual residuals are given in Eqs. (52) and (53). The iterative process terminates when both residuals fall below a sufficiently small

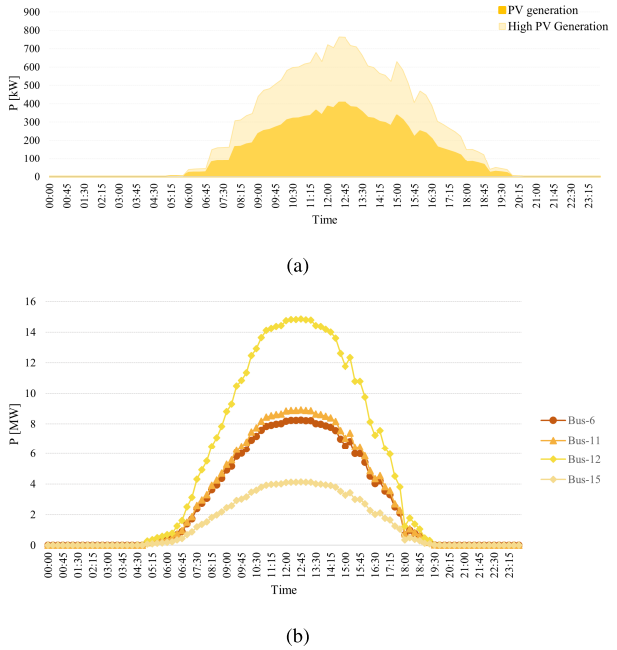

FIGURE 5. (a) Daily solar power generation profiles for PVs connected to the IEEE 33-Bus Network. (b) Daily solar power generation profiles for PVs connected to the Braintree Network.

threshold, ϵ, as specified in Eq. (54), indicating that a feasible stationary solution has been achieved.

$$r^k := \left[P_{i,t}^{\mathrm{DG},k} - P_{i,t}^{\mathrm{DS},k}, Q_{i,t}^{\mathrm{DG},k} - Q_{i,t}^{\mathrm{DS},k}\right] \tag{52}$$

$$s^k := \left[\rho\left(P_{i,t}^{\mathrm{DG},k+1} - P_{i,t}^{\mathrm{DG},k}\right), \rho\left(P_{i,t}^{\mathrm{DS},k+1} - P_{i,t}^{\mathrm{DS},k}\right), \rho\left(Q_{i,t}^{\mathrm{DG},k+1} - Q_{i,t}^{\mathrm{DG},k}\right), \rho\left(Q_{i,t}^{\mathrm{DS},k+1} - Q_{i,t}^{\mathrm{DS},k}\right)\right] \tag{53}$$

$$\|r^k\|_2 \leq \epsilon \quad \text{and} \quad \|s^k\|_2 \leq \epsilon \tag{54}$$

III. NUMERICAL RESULTS AND DISCUSSION

A. INPUT DATA

The proposed algorithm is firstly implemented on the customized IEEE 33-Bus Distribution Test System [32], incorporating real power demand data obtained from Iowa DS smart meter readings [33]. To assess the impact of distributed generation on operational constraints, PV systems are connected at the end of the feeder at Bus-16 and Bus-17 in the IEEE 33-bus test system, hereafter referred to as DG-1 and DG-2, respectively. Power generation data for a summer period is sourced from [34] and is uniformly applied across both PV systems. For further analysis of the efficacy, a high PV generation scenario is considered, and the algorithms are compared. PV generation under normal and high generation conditions is visually represented in Fig. 5(a). The analysis is then extended to a real distribution network, the Braintree 33 kV system operated by UK Power Networks, with assumed locations for PV units and a BESS. To reflect future multi-energy system characteristics, the network is further enhanced by integrating an electrolyzer unit, as illustrated in Fig.4. The corresponding generation profiles for a representative summer period are derived from historical Great Britain generation data published by the National Energy System Operator [35]. The respective generation profiles for each PV is illustrated in Fig.5(b). A proton exchange membrane hydrogen generation system is selected [36], and the number of electrolyzers is set to three based on the hydrogen demand. Each electrolyzer has a net hydrogen production rate of 492 Nm^3/h, and its power consumption at full capacity is 4.7 kWh/Nm^3. The electrolyzer unit is located to supply hydrogen for tube trailers, which transport the hydrogen to a depot serving fuel cell buses operating in London [37]. The hydrogen demand for the tube trailers is determined based on the specifications of the fuel cell buses, as well as their routes and operational schedules. The capacity of the HSU is selected as 530 kg and is scaled in proportion to the electrolyzer capacity, as done in [38]. The minimum hydrogen level of the HSU is set to 165 kg to ensure that sufficient hydrogen is available to supply at least one tube trailer. The capacity of the BESS is set to 6 MWh based on real network data. The algorithm is evaluated in a Python environment using the Gurobi commercial solver. The optimization is performed over a 24-hour horizon with a time resolution of 15 minutes for each computation interval.

B. SIMULATION AND RESULTS

1) IEEE 33-BUST DISTRIBUTION TEST SYSTEM

To evaluate the effect of distributed-based adaptive Volt/VAr control algorithm, multiple cases are considered including centralised-based algorithms with adaptive Volt/VAr control and distributed-based algorithm with fixed Volt/VAr control:

- *Case-1:* A centralized AC OPF approach is employed, where the DS operator acts as the central controller with access to all DS information, including data from the PV systems. The AC OPF is executed with the objective of minimizing active power losses across the network while dynamically adjusting the voltage settings of the Volt/VAr control.
- *Case-2:* Similar to Case-1, the DS operator operates as the central controller, accessing all information concerning the DS, including DGs. However, in this scenario, its objective function shifts towards minimizing active power curtailment of PVs.
- *Case-3:* In this scenario, the DS operator and two PV systems are modeled as three distinct agents, each with its own objective. The DS operator focuses on minimizing active power losses across the network, using ACOPF to meet its objective while adhering to network operational constraints. Meanwhile, each PV system aims to minimize its own active power curtailment by dynamically adjusting the voltage settings of its Volt/VAr control. Unlike previous cases that rely on centralized decision-making, this approach allows each agent to independently determine its own decisions. Convergence across the agents is achieved

TABLE 1. Dynamic behavior of active power curtailment, Active power injection, and reactive power injection for PV systems on Bus-16 and Bus-17 across all cases.

	Nominal PV Generation				High PV Generation			
	Case 1	Case 2	Case 3	Case 4	Case 1	Case 2	Case 3	Case 4
Total Active Power Curtailment [MW]	2.551	0	1.103	1.307	19.264	1.060	16.032	15.942
Bus 16	0	0	0.050	0.060	3.003	0.061	6.441	6.347
Bus 17	2.551	0	1.050	1.246	16.260	1.003	9.594	9.594
Total Active Power Injection [MW]	21.181	22.607	22.279	22.252	25.264	40.336	28.209	28.069
Bus 16	11.866	11.289	11.604	11.722	19.262	20.657	15.678	15.666
Bus 17	9.315	11.318	10.675	10.531	6.002	19.679	12.529	12.403
Total Reactive Power Injection [MVAr]	0.084	-5.395	-3.559	-2.699	0.015	-15.213	-3.174	-6.045
Bus 16	0.040	-2.752	-1.998	-1.323	0.002	-7.494	-1.657	-2.970
Bus 17	0.045	-2.643	-1.561	-1.376	0.013	-7.719	-1.514	-3.075
Total Active Power Loss [MW]	2.978	3.185	3.090	3.059	2.856	4.085	2.969	3.139
Total Reactive Power Loss [MVAr]	2.003	2.173	2.093	2.070	1.937	3.019	2.040	2.170

through the iterative exchange of dual variables, utilizing a distributed optimization framework.

- *Case-4:* Similar to Case-3, the decision variables for the three agents—the DS operator and two DGs—are determined in a distributed manner. However, in this scenario, the DGs utilize Volt/VAr control with the default settings prescribed by the IEEE standard 1547, rather than the optimal voltage settings employed in Case-3. This distinction highlights the impact of using standard versus optimized settings on the performance of the distributed optimization framework.

Table 1 presents the numerical results across all cases under nominal and high PV generation scenarios, with the corresponding generation profiles illustrated in Fig. 5(a). The evaluation of the proposed distributed algorithm and its comparison with centralized approaches are illustrated through time-varying dynamics in Figs. 6 - 9. Fig. 6 and Fig. 7 represent centralized methods. To assess the effect of the distributed approach, Fig. 8 highlights the impact of adaptive Volt/VAr control settings, while Fig. 9 compares it with the distributed algorithm using default Volt/VAr settings, providing a broader evaluation of the differences between default and adaptive control strategies. Moreover, Fig. 10(a) illustrates the total curtailment, active and reactive power injection, and network losses over a full day, providing an overall comparison across the simulation period. For a more

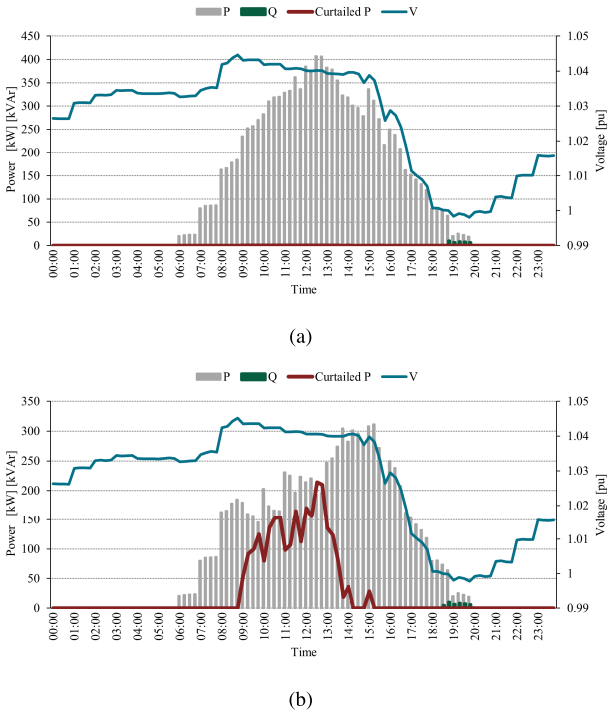

FIGURE 6. (a) Dynamic behaviour of active power curtailment, Active power injection, and Reactive power injection for DG-1, Alongside bus voltage (Case-1) (b) Dynamic behaviour of active power curtailment, Active power injection, and Reactive power injection for DG-2, Alongside bus voltage (Case-1).

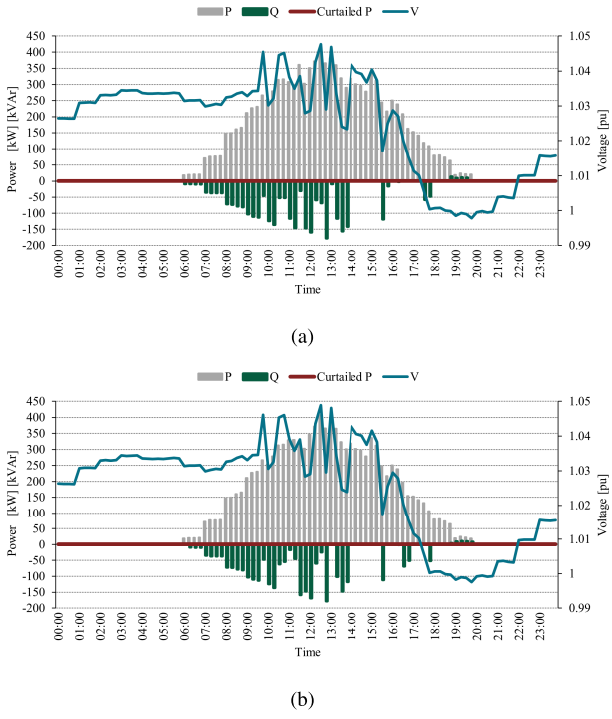

FIGURE 7. (a) Dynamic behaviour of active power curtailment, Active power injection, and Reactive power injection for DG-1, Alongside Bus Voltage (Case-2) (b) Dynamic behaviour of active power curtailment, Active power injection, and Reactive power injection for DG-2, Alongside bus voltage (Case-2).

in-depth analysis, Fig. 10(b) evaluates a high PV penetration scenario, offering a further comparison of all cases to assess the performance of the algorithms under more challenging conditions.

The time-varying active and reactive power allocation for DG-1 and DG-2 is illustrated Fig. 6. Reactive power is barely utilized for both DGs when the objective is to minimize power loss, as excessive reactive power increases network losses. Among all cases, Case-1 achieves the lowest active and reactive power losses at 2.978 MW and 2.003 MVAr, respectively, as shown in Figure 10(a). However, the limited use of reactive power leads to the highest curtailment, with a total of 2.5 MW curtailed, representing 21.5% of DG-2's generation, as depicted in Figure 10(a). Fig. 7 depicts the dynamics under Case-2, where the objective is to minimize curtailment. Reactive power absorption is allocated during periods of PV generation, successfully eliminating curtailment. However, focusing solely on minimizing curtailment results in excessive reactive power absorption, leading to significant voltage profile fluctuations for both DGs, as shown in Fig. 7(a) and Fig. 7(b). Furthermore, as illustrated in Fig. 10(a), this case yields the highest active and reactive power losses among all scenarios, with losses reaching 3.185 MW and 2.173 MVAr, respectively.

It is observed that utilizing reactive power significantly affects curtailment and network losses. Therefore, it must be carefully allocated, as the DS operator must efficiently manage the DS while minimizing curtailment to support DG owners and reduce environmental impact. In Case-3, the proposed distributed optimization-based algorithm facilitates the attainment of optimal solutions for each agent—comprising the DS operator and DG owners—by achieving convergence through the consideration of each agent's objective function and individual decisions. The distributed algorithm with adaptive Volt/VAr settings, illustrated in Fig. 8, shows a balanced performance. Compared to Case-1, it achieves lower curtailment, while the reactive power absorption is significantly reduced compared to Case-2. This results in less voltage deviation at DG-connected buses and lower curtailment, with 0.05 MW for DG-1 and 1.05 MW for DG-2. Fig. 9 illustrates the scenario where default Volt/VAr settings, as recommended by the standard, are used with the distributed approach instead of the adaptive settings applied in Case-3. When default Volt/VAr settings are employed, curtailment increases compared to Case-3, reaching 0.06 MW for DG-1 and 1.246 MW for DG-2.

Although Fig. 8 and Fig. 9 exhibit similar profiles, their efficiency differs significantly under high PV penetration, as shown in Fig. 10(b). The proposed adaptive Volt/VAr settings in Case-3 outperform the default Volt/VAr settings in Case-4 in terms of reducing network power loss. Specifically, Case-3 results in active and reactive power losses of 2.969 MW and 2.040 MVAr, respectively, whereas Case-4 causes 3.139 MW and 2.170 MVAr of active and reactive

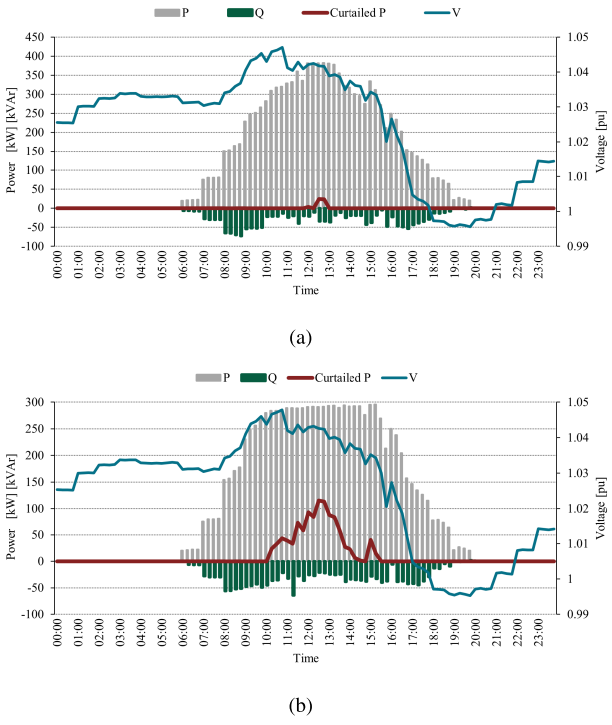

FIGURE 8. (a) Dynamic behaviour of active power curtailment, Active power injection, and Reactive power injection for DG-1, Alongside bus voltage (Case-3) (b) Dynamic behaviour of active power curtailment, Active power injection, and Reactive power injection for DG-2, Alongside bus voltage (Case-3).

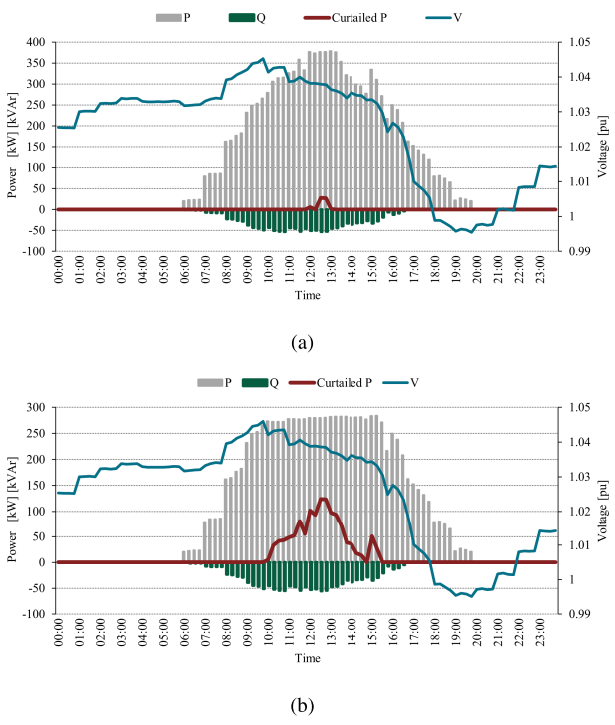

FIGURE 9. (a) Dynamic behaviour of active power curtailment, Active power injection, and Reactive power injection for DG-1, Alongside Bus Voltage (Case-4) (b) Dynamic behaviour of active power curtailment, Active power injection, and Reactive power injection for DG-2, Alongside bus voltage (Case-4).

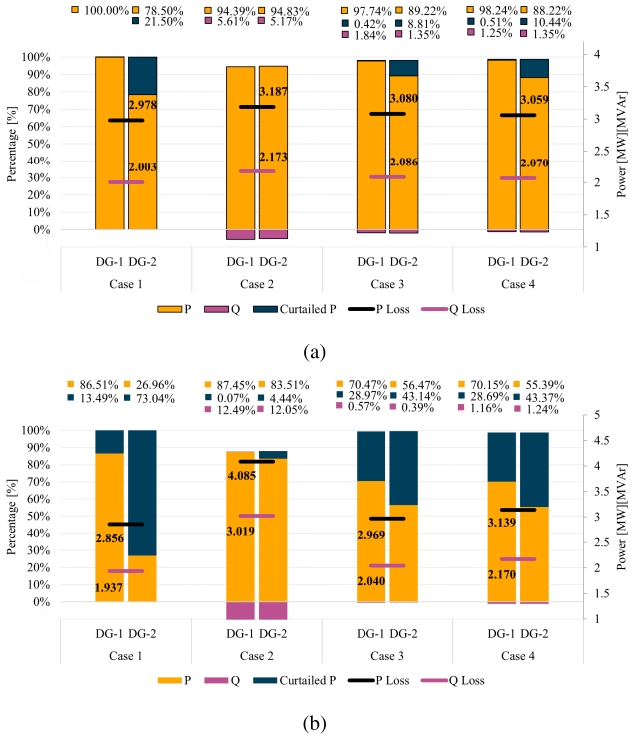

FIGURE 10. Comparison of power curtailment, Active and Reactive power allocation, and Network losses: (a) Full-Day Analysis and (b) High PV Penetration Scenario (Columns Represent Active and Reactive Power Allocation—Positive for Injection, Negative for Absorption; Lines represent total power loss).

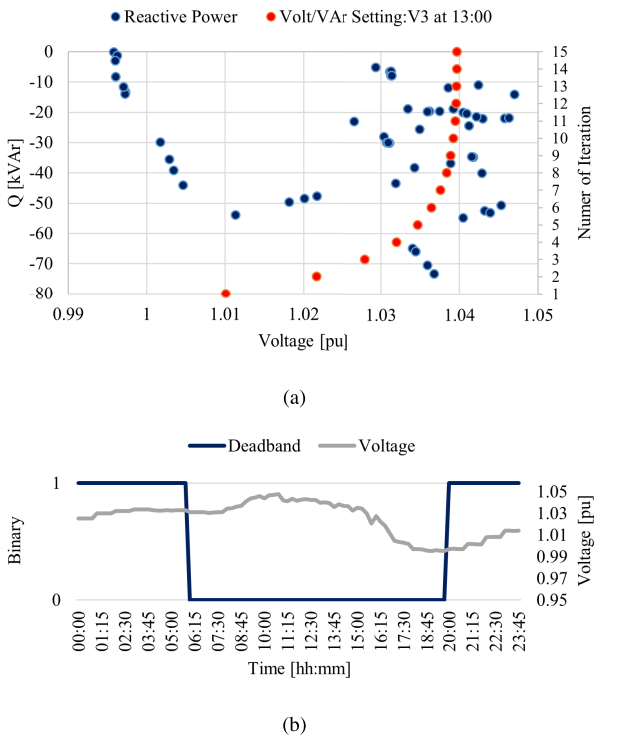

FIGURE 11. Adaptive Volt/VAr settings in Case-3 under normal PV generation conditions for DG-2: (a) v_3 variable settings and corresponding reactive power injection/absorption (positive for injection, negative for absorption), (b) Deadband activation over time and voltage profile.

TABLE 2. Overview of case studies: Objectives, Volt/VAr control approaches, and key outcomes.

Case	Objective: Minimization	Communication	Volt/VAr Control	Main Outcome
Case-1	Loss	Centralized	Adaptive Volt/VAr Control	Minimum loss; higher curtailment
Case-2	Curtailment	Centralized	Adaptive Volt/VAr Control	Zero curtailment; higher losses
Case-3	Loss and Curtailment	Distributed	Adaptive Volt/VAr Control	Balanced performance; improved voltage
Case-4	Loss and Curtailment	Distributed	Volt/VAr Control with Default Settings	Higher losses/curtailment; less efficient

power losses, despite providing similar curtailment. These results demonstrate that the proposed algorithm in Case-3 achieves approximately 5.41% and 6.00% reductions in active and reactive power losses, respectively. When comparing power and loss dynamics across the four cases under high PV generation, as shown in Figure 10(b), Case-1 achieves the minimum power loss at 2.856 MW and 1.937 MVAr by executing centralized AC OPF with the objective of minimizing power loss. However, no reactive power is allocated in this case, leading to the highest curtailment rates, with 13.49% and 73.04% of DG-1 and DG-2 PV generation curtailed, respectively. Conversely, the centralized algorithm with curtailment minimization achieves the lowest curtailment, with only 0.07% and 4.44% of DG-1 and DG-2 generation curtailed. However, this comes at the cost of excessive reactive power absorption, resulting in the highest power losses, 4.085 MW and 3.019 MVAr.

Comparing centralized and distributed algorithms, the distributed algorithms provide a balanced solution, considering both curtailment and power loss minimization. Among them, the proposed distributed algorithm with adaptive Volt/VAr settings outperforms the default settings by eliminating unnecessary reactive power absorption, with only 0.57% and 0.39% of DG-1 and DG-2 PV generation absorbed as reactive power. This reduction in reactive power absorption results in lower network losses compared to the default settings, while allowing for higher active power injection into the DS, 70.47% and 56.47% of DG-1 and DG-2 PV generation, respectively. Table 2 summarizes the performance of the proposed centralized and distributed control strategies under different objective functions and Volt/VAr settings.

A detailed analysis of the voltage setting decisions for DG-2 made by the proposed adaptive Volt/VAr algorithm is shown in Figs. 11 and 12. Fig. 11 presents the v_3 setting, reactive power absorption, voltage profile, and deadband duration under normal PV generation, while Fig. 12 shows these profiles under high PV generation. By examining the voltage profiles in Fig. 11(b) and Fig. 12(b), the voltage begins to rise with the PV generation. This increase is more significant under high PV generation, causing the deactivation of the deadband and triggering reactive power absorption. As shown in Figs. 11(a) and 12(a), reactive

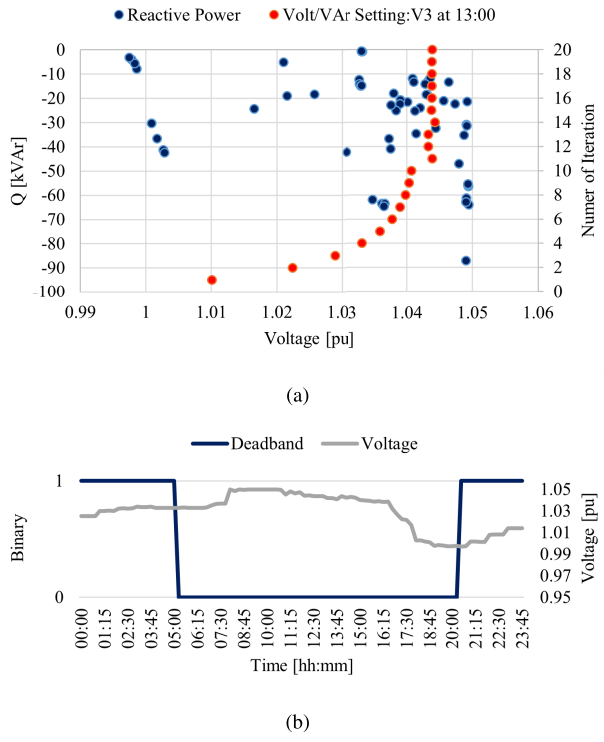

FIGURE 12. Adaptive Volt/VAr settings in Case-3 under high PV generation conditions for DG-2: (a) v_3 variable settings and corresponding reactive power injection/absorption (positive for injection, negative for absorption), (b) Deadband activation over time and voltage profile.

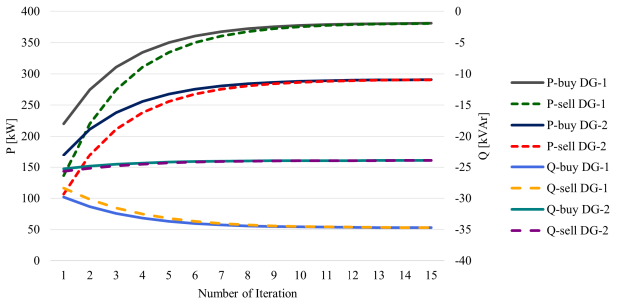

FIGURE 13. Convergence of adjacent variables at time 12:30 throughout 15 iteration.

power absorption increases with rising voltage, peaking in Fig. 12(a) when the voltage approaches the 1.05 pu limit. These results confirm that adaptive reactive power allocation effectively prevents voltage violations, ensuring stable and reliable network operation.

Figs. 11(a) and 12(a) illustrate the evolution of the v_3 setting at 13:00 across iterations. As shown in Fig. 11(a), following the initial step, the value converges to its final setting in fewer than 10 iterations and remains stable thereafter. A similar convergence pattern is observed in Fig. 12(a) under high PV generation conditions. It is worth noting that, in the high generation scenario, convergence requires approximately 15 iterations, reflecting the increased system stress and the more challenging coordination required to satisfy voltage constraints.

These results highlight the superior efficiency of the proposed distributed adaptive Volt/VAr control compared to distributed default Volt/VAr settings and centralized approaches. Fig. 13 analyzes the convergence performance of the proposed algorithm, showing the convergence of adjacent variables at 12:30, when PV generation is at its peak, across multiple iterations. With two DG connections in the network, active and reactive power allocation—treated as adjacent variables—is determined iteratively. Solid lines represent the DS operator agent's decisions, while dashed lines indicate the DG agents' decisions. The variables nearly converge within eight iterations, satisfying the convergence criterion in fewer than ten iterations.

Fig. 14 illustrates the evolution of voltage magnitude and reactive power for DG-1 and DG-2 across iterations, highlighting the convergence behaviour of the proposed distributed algorithm. For both DG units, the most notable variations occur during high PV generation periods, particularly between 08:00 and 18:00.In the initial iterations (approximately iteration 1 to 5), voltage levels exhibit visible fluctuations. This is primarily due to the initialization of the algorithm, where variables start from predefined initial values and progressively adjust towards the optimal solution. However, as the iterations progress, the voltage values stabilise and converge within a narrow band, remaining within the operational limits. This indicates that the algorithm effectively coordinates the control actions to achieve a consistent voltage profile across the network.

A similar convergence pattern is observed for reactive power. During the early iterations, up to iteration 5–8, significant fluctuations occur, especially in the same high generation window (08:00–18:00), where reactive power absorption reaches its highest levels, up to approximately -80 kVAr. As the iterations progress, these fluctuations diminish, and reactive power values converge to steady levels after approximately 10–15 iterations. During low generation periods, reactive power remains close to zero across all iterations, indicating minimal need for voltage support. Overall, convergence is consistently achieved within 10–15 iterations for both DG-1 and DG-2 across all time steps. This demonstrates the efficiency and robustness of the proposed distributed algorithm in coordinating voltage regulation and reactive power support under varying operating conditions.

2) BRAINTREE 33KV DISTRIBUTION NETWORK

To further evaluate the performance of the proposed algorithm, it is applied to a real distribution network comprising both standalone PV units and PV systems integrated with an electrolyzer and a BESS. Specifically, two standalone PV units are connected at Bus-6 and Bus-12, whose active and reactive power outputs are controlled in a distributed manner and modelled as independent DG agents. In contrast, the PV systems connected at Bus-15 and Bus-11 are integrated with an electrolyzer and a BESS, respectively, and are assumed to be owned and operated by the DS operator. Consequently, the active and reactive power allocation of these units is centrally

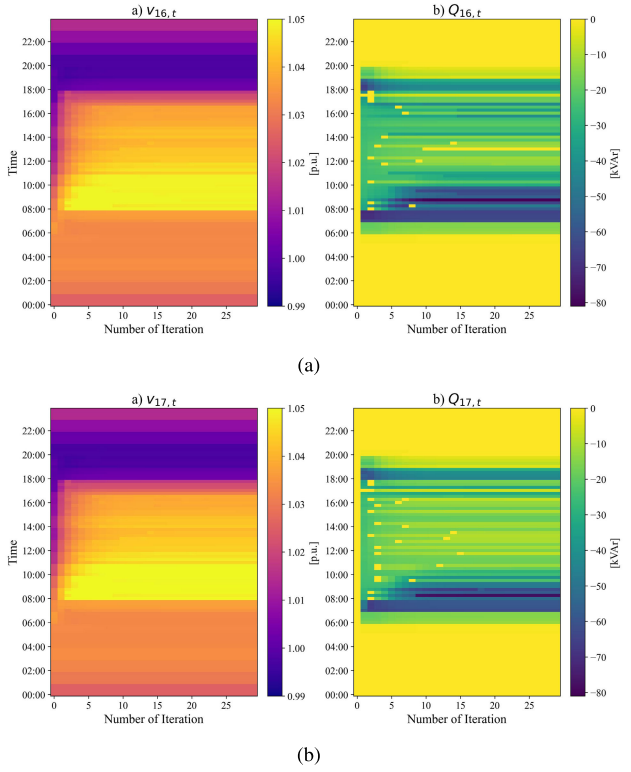

FIGURE 14. Convergence behaviour of voltage and reactive power under high PV generation conditions: (a) DG-1 and (b) DG-2.

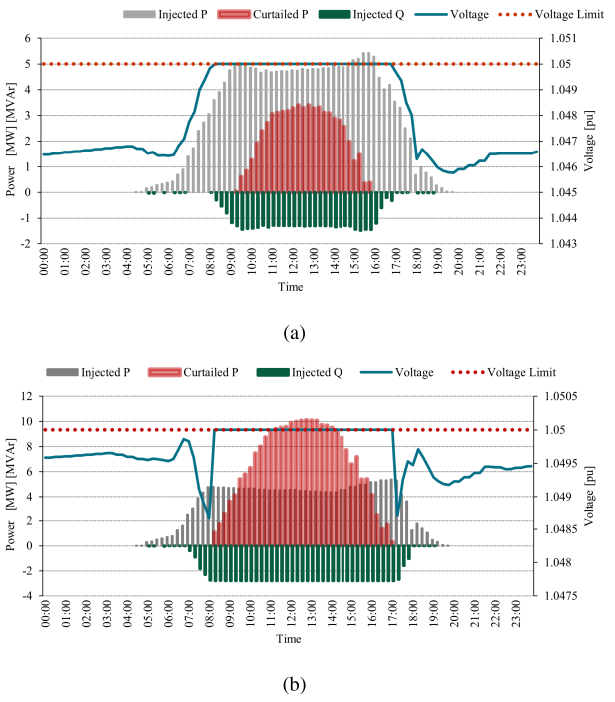

FIGURE 15. Dynamic behaviour of active power curtailment and active power injection alongside bus voltage profile.(a) for DG connected at Bus-6, (b) for DG connected at Bus-12.

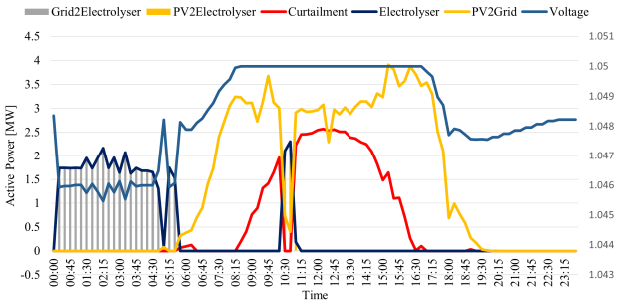

FIGURE 16. Dynamic behaviour of active power flow and voltage profile at Bus-15 where an hydrogen production plant and HSU is located.

managed by the DS agent. As detailed in Case-3, the objective of the DS agent is minimizing the power loss within the network and each DG agent aims to minimize their own PV curtailment.

The dynamic behaviour of active and reactive power flow adjustments under the proposed distributed control strategy is illustrated in Figs. 15(a) and Fig. 15(b). Since each agent operates locally with the objective of minimizing active power curtailment, reactive power support is not utilized before 08:00, as low PV generation does not lead to any violation of operational constraints, particularly voltage limits. As PV generation increases and voltage levels begin to rise, reactive power absorption is activated to maintain voltages within permissible limits and avoid curtailment. However, during periods of high PV generation, reactive power absorption alone becomes insufficient to regulate voltage, leading to the initiation of active power curtailment. For the PV unit connected to Bus-6, the total curtailed active power is 62.243 MW, while 41.883 MVAr of reactive power is absorbed, and 196.236 MW of active power is injected into the network. Similarly, for the PV unit connected to Bus-12, total active power curtailment reaches 242.569 MW, with 114.559 MVAr of reactive power absorbed and 213.532 MW of active power injected into the network.

Fig. 16 illustrates the active power dynamics at Bus-15, where an electrolyzer unit is connected alongside the HSU. During the period from midnight to the early morning hours, when PV generation is unavailable, the electrolyzer power demand reaches its highest level. This behaviour is driven by the requirement to satisfy hydrogen demand in advance of scheduled tube trailer departures. During periods of PV generation, however, the utilization of solar power for electrolyzer operation is minimal. As shown in Fig. 16, the hydrogen level in the HSU is maintained at its minimum operating threshold of 165 kg throughout this period. Instead of being consumed locally by the electrolyzer, the majority of the generated solar power is injected into the grid, with the remaining excess curtailed. This operational behaviour reflects the objective of the DG agent, which prioritizes minimization of network losses rather than maximization of renewable energy utilization or curtailment reduction.

Fig. 17 illustrates the active power dynamics at Bus-11, where a PV system operates in conjunction with an BESS. The charging and discharging behaviour of the BESS is influenced by the demand profile at Bus-10, which is located

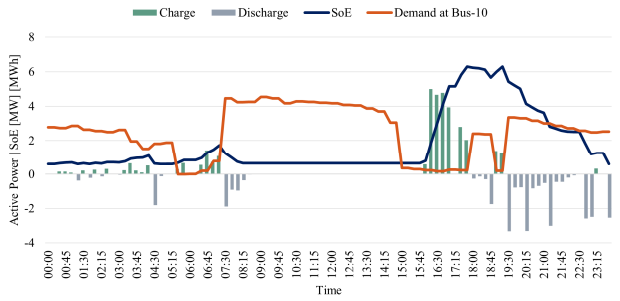

FIGURE 17. Charging and discharging power and state of energy of the BESS connected at Bus-11.

on the same feeder, as shown in Fig. 4. Since the objective of the DSO agent is to minimize network power losses, the BESS supports local demand by discharging when sufficient stored energy is available and charges during periods of lower demand. As observed in the figure, during high demand periods between 07:30 and 15:00, the BESS does not supply power because its state of energy reaches the minimum limit. Additionally, charging is not initiated during this period, as doing so would increase network losses. When demand decreases between 15:00 and 17:15, the BESS enters charging mode. The stored energy is then utilized to support demand during the remaining hours of the day.

IV. CONCLUSION

This study set out to develop a solution to address the growing complexity of DSs caused by the increasing penetration of DGs. Recognising real-life limitations in DS operations, where the DS operator has no direct control over DGs beyond their connectivity, and taking into account privacy concerns, this research is the first to propose a decision-making algorithm that addresses these practical constraints. The proposed distributed algorithm models the DS operator and DGs as distinct agents with separate objectives. The DS operator makes decisions based on its own objective function and the operational constraints of the network, while DGs, equipped with adaptive Volt/VAr control, aim to minimize their curtailment. Although each stakeholder operates independently, their decisions are coordinated in a distributed framework, ensuring convergence to a common solution that reflects both perspectives.

The algorithm is evaluated through a comprehensive comparison with centralized approaches under different objective functions, as well as with a distributed algorithm using default Volt/VAr settings. The performance of the method is validated on both the IEEE 33-bus distribution test system and a real-world network dataset, demonstrating its applicability across different system scales and levels of complexity. The real distribution network model includes an existing BESS and is further extended with an electrolyzer connection, enabling additional flexibility and the analysis of multi-energy system interactions. The results validate the effectiveness of the distributed approach, demonstrating its superiority over centralized methods by providing a balanced solution that considers the objectives of all stakeholders. The study also highlights the significant impact of reactive power allocation on DG curtailment and overall network operation. The proposed algorithm with adaptive Volt/VAr settings achieves 5.41% and 6.00% reductions in active and reactive power losses, respectively, compared to fixed Volt/VAr control. In short, it can be stated that this study makes a valuable contribution to the literature as the first to model real-world challenges in DSs, including privacy concerns and operational limitations in DG connections. The findings emphasize the critical role of distributed approaches and efficient reactive power allocation in achieving an optimized, efficient, and sustainable DS.

REFERENCES

[1] National Grid. (Dec. 2022). *Q-Flex Project: Reactive Power Technology Catalogue*. [Online]. Available: https://www.nationalgrid.co.uk/downloads-view-reciteme/626639

[2] SP Energy Networks. (2021). *Reactive Power Trial in Partnership With Conrad Energy*. [Online]. Available: https://www.spenergynetworks.co.uk/userfiles/file/March%2023%20-%20Reactive%20Power%20Trial.pdf

[3] U.K. Power Networks. (Aug. 2021). *Power Potential (Transmission & Distribution Interface 2.0) Project Close Down Report*. [Online]. Available: https://innovation.ukpowernetworks.co.uk/projects/power-potential

[4] Energy Networks Association. (Jul. 2024). *Q-Flex Project Summary*. [Online]. Available: https://smarter.energynetworks.org/projects/nia_wpd_072

[5] IEEE Standards Association and Institute of Electrical and Electronics Engineers. (2018). *IEEE Standard for Interconnection and Interoperability of Distributed Energy Resources With Associated Electric Power Systems Interfaces*. [Online]. Available: https://standards.ieee.org/ieee/1547/5915/

[6] Massachusetts Institute of Technology. (2011). *MIT Study on the Future of the Electric Grid*. [Online]. Available: https://energy.mit.edu/wp-content/uploads/2011/12/MITEI-The-Future-of-the-Electric-Grid.pdf

[7] Y. Gupta, S. Doolla, K. Chatterjee, and B. C. Pal, "Optimal DG allocation and volt–var dispatch for a droop-based microgrid," *IEEE Trans. Smart Grid*, vol. 12, no. 1, pp. 169–181, Jan. 2021.

[8] Z. Tang, D. J. Hill, and T. Liu, "Distributed coordinated reactive power control for voltage regulation in distribution networks," *IEEE Trans. Smart Grid*, vol. 12, no. 1, pp. 312–323, Jan. 2021.

[9] D. K. Molzahn, F. Dörfler, H. Sandberg, S. H. Low, S. Chakrabarti, R. Baldick, and J. Lavaei, "A survey of distributed optimization and control algorithms for electric power systems," *IEEE Trans. Smart Grid*, vol. 8, no. 6, pp. 2941–2962, Nov. 2017.

[10] N. Patari, V. Venkataramanan, A. Srivastava, D. K. Molzahn, N. Li, and A. Annaswamy, "Distributed optimization in distribution systems: Use cases, limitations, and research needs," *IEEE Trans. Power Syst.*, vol. 37, no. 5, pp. 3469–3481, Sep. 2022.

[11] W. Zheng, W. Wu, B. Zhang, H. Sun, and Y. Liu, "A fully distributed reactive power optimization and control method for active distribution networks," *IEEE Trans. Smart Grid*, vol. 7, no. 2, pp. 1021–1033, Mar. 2016.

[12] H. Li, K. Guo, G. Hao, M. Mao, and L. Zhou, "Decentralized communication based two-tier volt-var control strategy for large-scale centralized photovoltaic power plant," *IEEE Trans. Sustain. Energy*, vol. 13, no. 1, pp. 592–606, Jan. 2022.

[13] R. R. Jha, A. Dubey, T. Hong, and D. Zhao, "Distributed algorithm for volt–var optimization in unbalanced distribution system," in *Proc. IEEE Power Energy Soc. Innov. Smart Grid Technol. Conf. (ISGT)*, Feb. 2020, pp. 1–5.

[14] H. J. Liu, W. Shi, and H. Zhu, "Distributed voltage control in distribution networks: Online and robust implementations," *IEEE Trans. Smart Grid*, vol. 9, no. 6, pp. 6106–6117, Nov. 2018.

[15] B. Li and Q. Xu, "A machine learning-assisted distributed optimization method for inverter-based volt-var control in active distribution networks," *IEEE Trans. Power Syst.*, vol. 39, no. 2, pp. 2668–2681, Mar. 2024.

[16] T. Xu and W. Wu, "Accelerated ADMM-based fully distributed inverter-based volt/var control strategy for active distribution networks," *IEEE Trans. Ind. Informat.*, vol. 16, no. 12, pp. 7532–7543, Dec. 2020.

[17] Y. Guo, H. Gao, and Q. Wu, "Distributed cooperative voltage control of wind farms based on consensus protocol," *Int. J. Electr. Power Energy Syst.*, vol. 104, pp. 593–602, Jan. 2019.
[18] Interstate Renewable Energy Council (IREC), *Making the Grid Smarter: Primer on Adopting the New IEEE Standard 1547-2018*, Standard EEE Standard 1547-2018, 2018.
[19] International Trade Administration. (2021). *Smart Grid Interoperability Standards Adoption in Southeast Asia*. [Online]. Available: https://www.trade.gov/sites/default/files/2021-12/Smart%20Grid%20Interoperability%20Standards%20Adoption%20in%20Southeast%20Asia_Publication_508_Compliant.pdf
[20] G. C. Kryonidis, K.-N.-D. Malamaki, S. I. Gkavanoudis, K. O. Oureilidis, E. O. Kontis, J. M. Mauricio, J. M. Maza-Ortega, and C. S. Demoulias, "Distributed reactive power control scheme for the voltage regulation of unbalanced LV grids," *IEEE Trans. Sustain. Energy*, vol. 12, no. 2, pp. 1301–1310, Apr. 2021.
[21] H. Lee, J.-C. Kim, and S.-M. Cho, "Optimal volt–var curve setting of a smart inverter for improving its performance in a distribution system," *IEEE Access*, vol. 8, pp. 157931–157945, 2020.
[22] A. M. Howlader, S. Sadoyama, L. R. Roose, and S. Sepasi, "Distributed voltage regulation using volt-var controls of a smart PV inverter in a smart grid: An experimental study," *Renew. Energy*, vol. 127, pp. 145–157, Nov. 2018.
[23] D. Gebbran, S. Mhanna, A. C. Chapman, and G. Verbič, "Multiperiod DER coordination using ADMM-based three-block distributed AC optimal power flow considering inverter volt-var control," *IEEE Trans. Smart Grid*, vol. 14, no. 4, pp. 2874–2889, Jul. 2023.
[24] Y. Zeng, Y. Qiu, J. Zhu, S. Chen, B. Zhou, J. Li, B. Yang, and J. Lin, "Scheduling multiple industrial electrolyzers in renewable P2H systems: A coordinated active-reactive power management method," *IEEE Trans. Sustain. Energy*, vol. 16, no. 1, pp. 201–215, Jan. 2025.
[25] X. Zhang, C. Gu, H. Wang, G. Wang, Y. Xu, and A. R. Sayed, "Hydrogen energy storage system participated decentralized voltage control with multi-agent deep reinforcement learning method," *IEEE Trans. Ind. Appl.*, vol. 61, no. 2, pp. 2578–2588, Feb. 2025.
[26] D. A. Quijano, A. Padilha-Feltrin, and J. P. S. Catalão, "Volt-var optimization with power management of plug-in electric vehicles for conservation voltage reduction in distribution systems," in *Proc. IEEE Int. Conf. Environ. Electr. Eng. IEEE Ind. Commercial Power Syst. Eur.*, Jun. 2022, pp. 1–6.
[27] S. Gupta, A. Mehrizi-Sani, S. Chatzivasileiadis, and V. Kekatos, "Deep learning for scalable optimal design of incremental volt/var control rules," *IEEE Control Syst. Lett.*, vol. 7, pp. 1957–1962, 2023.
[28] S. Gupta, V. Kekatos, and S. Chatzivasileiadis, "Optimal design of volt/var control rules of inverters using deep learning," *IEEE Trans. Smart Grid*, vol. 15, no. 5, pp. 4731–4743, Sep. 2024.
[29] X. Sun, J. Qiu, Y. Tao, and J. Zhao, "Data-driven combined central and distributed volt/var control in active distribution networks," *IEEE Trans. Smart Grid*, vol. 14, no. 3, pp. 1855–1867, May 2023.
[30] X. Zheng, S. Yu, H. Cao, T. Shi, S. Xue, and T. Ding, "Sensitivity-based heterogeneous ordered multi-agent reinforcement learning for distributed volt-var control in active distribution network," *IEEE Trans. Smart Grid*, vol. 16, no. 3, pp. 2115–2126, May 2025.
[31] S. Boyd, N. Parikh, E. Chu, B. Peleato, and J. Eckstein, "Distributed optimization and statistical learning via the alternating direction method of multipliers," *Found. Trends Mach. Learn.*, vol. 3, no. 1, pp. 1–122, Jul. 2011.
[32] M. E. Baran and F. F. Wu, "Network reconfiguration in distribution systems for loss reduction and load balancing," *IEEE Trans. Power Del.*, vol. 4, no. 2, pp. 1401–1407, Feb. 1989.
[33] F. Bu, Y. Yuan, Z. Wang, K. Dehghanpour, and A. Kimber, "A time-series distribution test system based on real utility data," in *Proc. North Amer. Power Symp. (NAPS)*, Wichita, KS, USA, Oct. 2019, pp. 1–6.
[34] S. Pfenninger and I. Staffell, "Long-term patterns of European PV output using 30 years of validated hourly reanalysis and satellite data," *Energy*, vol. 114, pp. 1251–1265, Nov. 2016.
[35] (2025). *Historic Gb Generation Mix*. [Online]. Available: https://www.neso.energy/data-portal/historic-generation-mix/historic_gb_generation_mix
[36] NEL. (2024). *Electrolysers for High Purity Industrial Applications*. [Online]. Available: https://nelhydrogen.com/resources/proton-pem-electrolysers/
[37] (2024). *Improving Buses*. [Online]. Available: https://tfl.gov.uk/modes/buses/improving-buses
[38] J. Zhang, C. Li, G. Chen, and Z. Dong, "Planning of hydrogen refueling stations in urban setting while considering hydrogen redistribution," *IEEE Trans. Ind. Appl.*, vol. 58, no. 2, pp. 2898–2908, Mar. 2022.

HILAL OZDEMIR received the B.Sc. degree in control and automation engineering and the second B.Sc. and M.Sc. degrees in electrical engineering from Yıldız Technical University (YTU). She is currently pursuing the Ph.D. degree in electronic and electrical engineering with the Brunel University of London. Since 2024, she has been with UK Power Networks Distribution System Operator, where she works on the operation and development of smart, flexible, and resilient electricity distribution networks. Her work supports the integration of distributed energy resources and the transition toward low-carbon power systems in U.K. Her research interests include smart grids, renewable energy integration, distributed energy resources, and control and optimization of modern electrical networks.

A. SELIM TURKOGLU received the B.Sc. degree in electrical and electronics engineering from Koç University and the M.Sc. degree in electrical engineering from Yıldız Technical University. He is currently pursuing the Ph.D. degree in electrical engineering with the University of Porto. His research contributions include power systems, smart grids, distributed energy resources, and related control and optimization techniques. His current research interests include power system analysis, grid modernization, integration of renewable and distributed generation, and optimization of electrical networks.

OZAN ERDINÇ (Senior Member, IEEE) received the B.Sc., M.Sc., and Ph.D. degrees from Yıldız Technical University (YTU), Istanbul, Türkiye, in 2007, 2009, and 2012, respectively. Until May 2013, he was in the private sector in different positions, including electrical installations, renewable energy investments, and a procurement expert. In June 2013, he was a Postdoctoral Fellow in Portugal under the EU-FP7-Funded Singular Project. Afterwards, he joined YTU, where he is currently a Full Professor and the Head of the Department of Electrical Engineering. He was formerly the Head of the IT Department, YTU; the Director of the Energy Application and Research Center, YTU; and the Head of the Alternative Energy Based Electric Systems Division, Department of Electrical Engineering, YTU. He was the Editorial Board Member of IEEE TRANSACTIONS ON SUSTAINABLE ENERGY, IEEE OPEN ACCESS JOURNAL OF POWER AND ENERGY, IEEE SYSTEMS JOURNAL, *IET Smart Grid*, *IET Renewable Power Generation*, and *IET Generation, Transmission and Distribution*. He is currently the Editorial Board Member of IEEE ACCESS, IEEE TRANSACTIONS ON SYSTEMS, MAN, AND CYBERNETICS: SYSTEMS, IEEE TRANSACTIONS ON INTELLIGENT TRANSPORTATION SYSTEMS, and IEEE INTERNET OF THINGS JOURNAL.

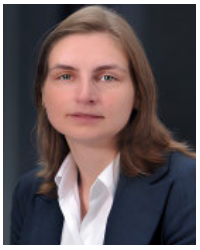

IOANA PISICA (Senior Member, IEEE) is currently an Associate Professor of power systems and a member of the Brunel Interdisciplinary Power Systems Research Centre, Brunel University of London. She has been involved in agent-based modeling, smart metering communications, and analysis of large amounts of data from smart meters, with the aim to achieve energy efficiency. Her research interests include power systems operation optimization, renewable energy systems, power quality, and energy efficiency in the built environment and industry. Her expertise in building management systems and energy management systems spans across more than 12 years.